# Resource-saving circulating pump through optimization of the integrated canned motor

Juri Dolgirev*, Marc Kalter*, Volker Schimmelpfennig*, Ralph Funck, Jens Jung**, Sven Urschel**
* Electrotechnical Systems in Mechatronics, University of Applied Sciences Kaiserslautern, Germany
* CirComp GmbH, Germany

## Abstract

A circulation pump is an integrated unit, consisting of a hydraulic part for transmitting energy to the medium and a driving canned electric motor. The strict efficiency standards for circulation pumps set by the European Union led to the fact, that today synchronous motor with cost-intensive and resource critical rare earth magnets are state of the art. This paper presents a new resource saving design for canned motors of circulation pumps based on a novel separation can in combination with a ferrite assisted synchronous reluctance motor.

## 1 Introduction

More than 140 million circulation pumps are installed in Europe alone [1]. Due to this high number of pumps used, the potential for CO2 reduction by increasing the energy efficiency of these pumps is correspondingly high. The motor used in circulation pumps is a so-called canned motor, which is surrounded by an electrically conductive liquid medium, typically water. Because the rotor of the motor is running wet, it is necessary to hermetically seal the stator winding against the pumped fluid. This is achieved by means of a separation can in the air gap between rotor and stator (**Figure 1**). Since significant eddy current losses occur in metallic cans [2], cans made of plastic are partially used today. To ensure the required compressive strength and diffusion resistance the cans made of plastic have to be much thicker. As a result, today´s circulating pumps are generally equipped with a permanent magnet motor with rare earth magnets and a motor-mounted frequency converter.

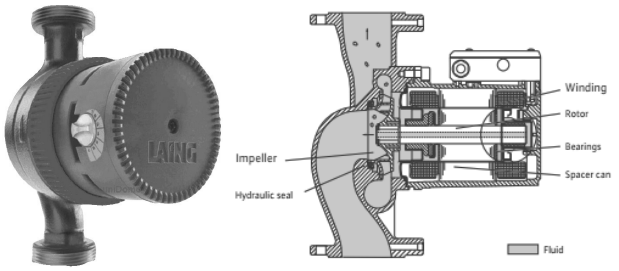


**Figure 1** Example of a circulation pump (left) and schematic illustration of such a pump (right) [3, 4]

The question to be answered in this paper is how rare-earth-free motors in circulation pumps could be used to achieve the efficiency standard set by the EU. The focus was on the development of an integrated ferrite assisted synchronous reluctance drive system. Due to its simple design, the synchronous reluctance motor (SynRM) provides an excellent basis for increasing the resource efficiency: In the rotor, neither copper windings nor rare earth magnets are needed, while the stator is designed as in a conventional synchronous machine. The use of a SynRM requires a non-metallic can with the thinnest possible wall thickness to minimize the air gap between stator and rotor. The approach followed here is based on a novel can made of a combination of carbon fiber reinforced plastic and polyphenylene sulfide.

## 2 Basic design of the considered electric motor and theoretical fundamentals

**Figure 2** shows on the left side a typical basic design of a four-pole synchronous reluctance machine without magnetic support. The stator is designed with 24 slots and has a distributed winding to reduce harmonics in the air gap magnetic field. The development of the internal torque is based on the reluctance principle through targeted flux guidance in the rotor, which is designed in the flux barrier shape.
The equation for the internal torque is given in (1). $L_d$ and $L_q$ as well as $i_d$ and $i_q$ are the inductances respectively the currents in the d- and q-axis. The equation (1) can be converted via (2) into the form of equation (3). It can be seen that the torque can be increased by varying the difference between the flux linkage $\Psi_d$ and $\Psi_q$. The internal torque thus becomes maximum if the flux linkage in q-direction approaches zero or if an additional flux acts against $\Psi_q$ and removes it.

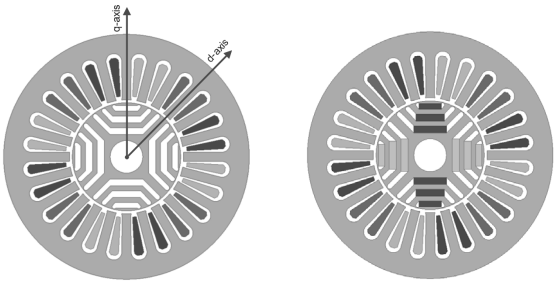


**Figure 2** Schematic representation of a synchronous reluctance motor (left) and a ferrite assisted synchronous reluctance motor (right)

$$M = \frac{3p}{2} L_q(i_d, i_q) \left[ \frac{L_d(i_d, i_q)}{L_q(i_d, i_q)} - 1 \right] i_d i_q \quad (1)$$

$$M = \frac{3p}{2} \left[ L_d(i_d, i_q) - L_q(i_d, i_q) \right] i_d i_q \quad (2)$$

$$M = \frac{3p}{2} \left[ \Psi_d i_q - \Psi_q i_d \right] \quad (3)$$

An oppositely directed magnetic flux in the q-axis can be achieved by using permanent magnets (**Figure 2, right**). The magnets should not generate the main flux in the rotor, but, as described above, counteract the flux linkage $\Psi_q$ and contribute to the increase of the torque. Here, well available and cheap ferrite magnets can be used instead of expansive rare earth magnets. This has a positive effect on the resource efficiency in pump drives. The phase diagram in **Figure 3** [5, 6] shows the influence of the ferrite magnets on the voltage and flux vectors. It can be seen that the resulting flux linkage $\Psi$ moves in the direction of the d-axis and with an optimal dimensioning and placement of the permanent magnets, the q-component can be completely eliminated. Despite the presence of magnets in the rotor, the electric machine is still regarded as a synchronous reluctance motor, but assisted with additional ferrite magnets (PMSynRM). The torque equation (6) of a PMSynRM can be derived by increasing the flux in the q-direction [6, 7, 8], $\Psi_q$ and $\Psi_m$ must be added (4).

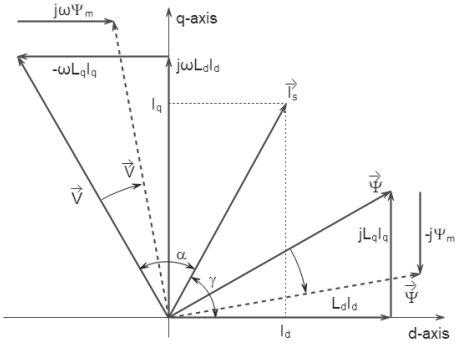


**Figure 3** Phase diagram of PMSynRM

$$\Psi_{q\_total} = \Psi_q + \Psi_m \quad (4)$$

$$M = \frac{3p}{2} \left[ \Psi_d i_q - (\Psi_q + \Psi_m) i_d \right] \quad (5)$$

$$M = \frac{3p}{2} \left[ \Psi_d i_q - \Psi_q i_d - \Psi_m i_d \right] \quad (6)$$

# 3 Numerical simulation

## 3.1 Torque and flux linkage

The correctness of equation (6) for the internal torque and thus the elimination of the flux in the q-direction can be verified by using numerical methods (e.g. finite element method). For this purpose, a simulation model was set up and the optimal placement of the ferrite magnets according to [9] was carried out. The simulation results are shown in **Figure 5**, **Figure 6** and **Figure 7**. **Figure 5** shows the individual flux linkages of the three winding strands of a SynRM as a function of the electrical angle. These must be transformed into d-q-coordinates as shown in **Figure 6**. The analysis of the curves must take into account the electrical angle for the maximum torque. **Figure 6** shows that the curve of the q-component must be shifted in a positive direction. Thus the internal torque can be increased with the same current supply to the motor. According to equation (6), this would mean that the flux concatenation $\Psi_m$ has the same amount as $\Psi_q$ and is opposite to it. **Figure 7** shows the curves of the flux linkages in d- and q-direction as well as the torque after which the flux barriers of the rotor were occupied with permanent magnets.

It can be seen that the curve for $\Psi_q$ has moved in the direction of the positive axis. At the current angle for the maximum torque, the value of the q-component is minimal. This has a positive effect on the development of the internal torque in the machine.

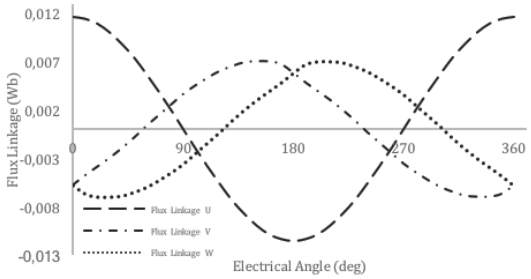


**Figure 4** SynRM: Flux linkage in Phases U, V, W

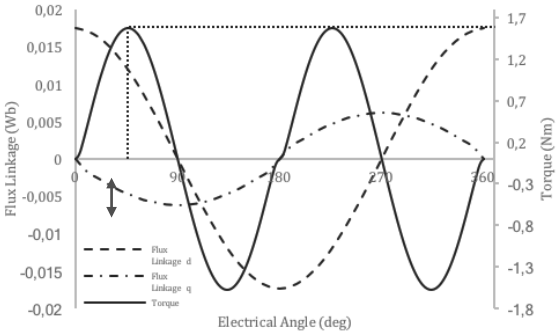


**Figure 5** SynRM: Torque and flux linkage in d- and q-axis

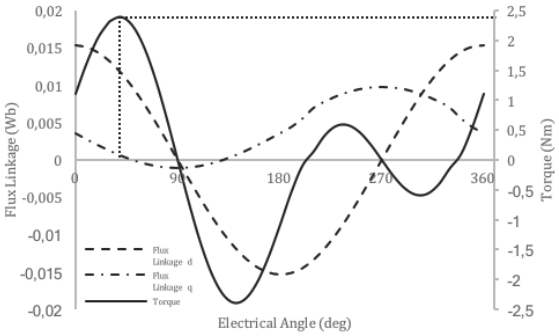


**Figure 6** PMSynRM: Torque and flux linkage in d- and q-axis

## 3.2 Comparison between SynRM and PMSynRM

In the simulation models, the same basic motor was used for both, SynRM and PMSynRM (**Figure 2**). To minimize the torque ripple, the rotor was staggered and divided into

three segments. The stator and rotor geometries are identical in both models, with the difference that in PMSynRM the flux barriers are equipped with permanent magnets (Table 1). **Figure 7** shows the simulated torque curves in the steady state at 3200 rpm. By using the permanent magnets, the torque and thus the mechanical power of the electric machine could be increased by 33 %.

**Table 1** Data of the simulation models

| Data | SynRM | PMSynRM |
|---|---|---|
| Current (A) | 4 | 4 |
| Length (mm) | 56 | 56 |
| Stator diameter (mm) | 105 | 105 |
| Rotor diameter (mm) | 46,3 | 46,3 |
| Air gap width (mm) | 1,25 | 1,25 |
| Slot number | 24 | 24 |
| Number of magnets | 0 | 36 |
| Winding | Distributed winding | Distributed winding |
| Rotor staggered | 3 segments | 3 segments |
| Torque (Nm) | 1,58 | 2,40 |

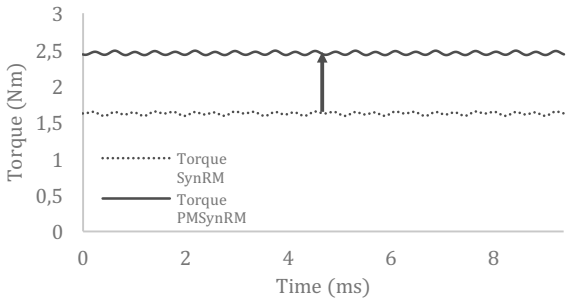


**Figure 7** Torque curve in steady state condition

# 4 Development of the can

## 4.1 Torque Reduction by increased air gap

A circulating pump is used to transport a medium between a heat generator and a heat consumer. The typical structure of such pumps is shown in **Figure 8**. The impeller of the pump is driven by an electric motor. Stator and rotor are, as already mentioned, separated by a can. This can is located in the air gap and hermetically isolates the stator from the liquid flowing around in the rotor chamber.

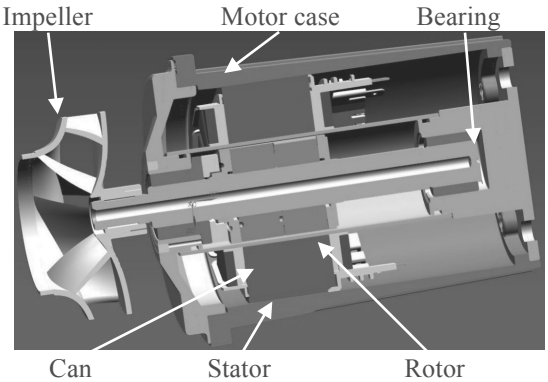


**Figure 8** 3d model of a circulating pump

The can leads to an enlarged air gap which results in SynRM in a reduced torque per ampere under otherwise similar conditions. As shown in **Figure 9** the internal torque of a standard SynRM drops rapidly as a function of the air gap width. According to (1) this behaviour can be explained by the ratio of the d-axis and q-axis inductances $L_d$ and $L_q$. An enlarged air gap results especially in a strong decreased $L_d$ (**Figure 10**), which leads to a reduced ratio of $L_d$ and $L_q$ (**Figure 11**) and thereby to a reduced internal torque. For this reason, the minimum achievable wall thickness is of great importance in can development. In order to avoid eddy current losses, the can should have no electrical conductivity. Thus, the energy efficiency of the motor and the entire pump unit can be improved.

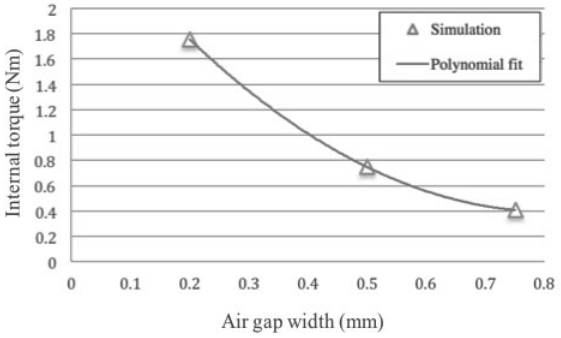


**Figure 9** Internal torque at rated current and rated speed in dependence upon air gap width

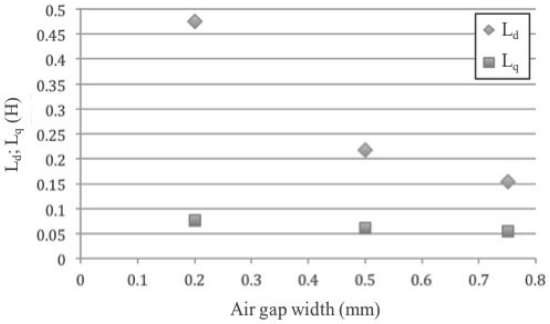


**Figure 10** FEM simulated $L_d$ and $L_q$ at rated current in dependence upon air gap width

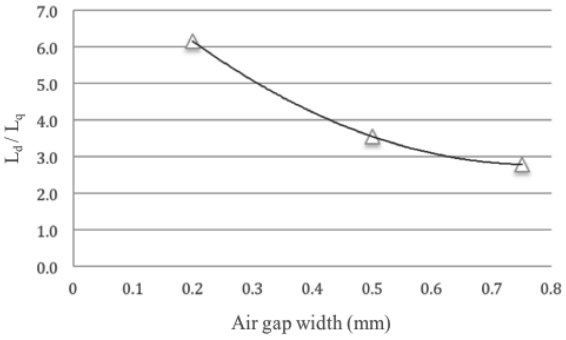


**Figure 11** Ratio of $L_d$ and $L_q$ at rated current in dependence upon air gap width

## 4.2 Specification of the can

The can is exposed to high pressures and temperatures, is subject to pressure and temperature fluctuations and must

also have high media resistance. Depending on the application, even drinking water approval is required. **Table 2** lists the most important requirements for the can.

**Table 2** Specification of the can

| Features | Heating water | Drinking water |
|---|---|---|
| System pressure (bar) | 16 | 10 |
| Burst pressure (bar) | 24 | 15 |
| Temperature of the pumping medium (°C) | -10 - 110 | |
| Material | Non-metallic | |

## 4.3 Manufacturing technology

Various concepts for the production of fibre composite cans were developed and compared for the development of the can. In principle, the can consists of a media-conducting inner layer (liner) and a reinforcement produced by the fibre winding process with carbon fibres running continuously in the circumferential direction. The liner can protect the inside of the can against aggressive media and guarantees the tightness of the can better than the fibre composite [10]. Due to the carbon fibres running in the circumferential direction, a particularly high compressive strength is achieved for the can even at low CFRP (carbon fiber-reinforced polymer) wall thicknesses.

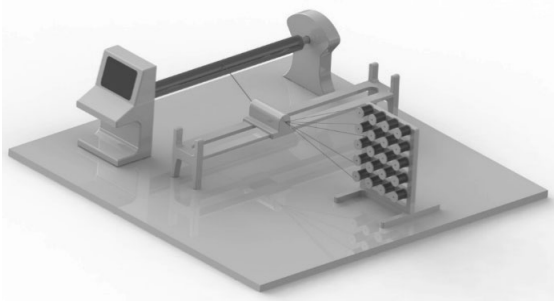

**Figure 12** Filament winding technology

### 4.3.1 Concept 1a – Pressing a CFRP roll onto an injection-moulded liner

In this already established concept, a thin-walled injection-moulded pipe is produced as a diffusion-proof liner. A thin-walled CFRP sleeve manufactured using fiber winding technology serves as a pressure-resistant layer on the outside. Both components are manufactured independently of each other and the CFRP sleeve is then pressed onto the injection-moulded pipe. The main challenges of this concept are the demoulding of the thin-walled injection-moulded part and the possible damage to one of the two components during pressing.

### 4.3.2 Concept 1b – Direct winding of an injection-moulded liner

This concept also uses a thin-walled injection-moulded pipe as a diffusion-tight liner. The injection-moulded pipe is picked up in a winding tool and then wound with CFRP layers to ensure the pressure resistance of the can. In addition to the already mentioned demoulding of the thin-walled injection-moulded part, its handling during direct winding represents a challenge for the concept.

### 4.3.3 Concept 1c – Back injection of a CFRP pipe

This concept is based on a thin-walled CFRP winding part. In a further step, the CFRP roll is positioned in an injection mould and back-moulded with a thermoplastic on the inside of the tube. The thermoplastic thus forms a diffusion-tight liner. While concepts 1a and 1b provide for a CFRP roll with an epoxy resin matrix, this would be problematic in this case because the temperature resistance of the epoxy resin (140 °C) is significantly below the processing temperature of potential liner thermoplastics (e.g. PPS: 310 °C - 340 °C; PA6: 270 °C - 295 °C [11]). For this reason, concept 1c provides for a CFRP wrap with a thermoplastic matrix. One hurdle with this concept is the increased material and processing costs to produce thermoplastic CFRP pipes.

### 4.3.4 Concept 2 – Internal coating of a CFRP pipe

A thin-walled CFRP winding part with an epoxy resin matrix as a pressure-resistant outer layer serves as the starting point. A plastic coating is applied to the inside of this winding part by hot pressing. The challenges of this concept lie in the uniform application and sufficiently strong adhesion of the diffusion-tight inner coating to the CFRP winding part.

## 4.4 Comparison of concepts

The concepts 1a-c have in common that the diffusion-tight liner inside is realized by an injection-moulded pipe. Compared to concept 2, where the diffusion barrier is implemented by a thin-walled coating, concepts 1a-c are expected to have an increased wall thickness due to the additional component. Production results to date show that wall thicknesses of the injection-moulded liner alone of less than 0.7 mm are difficult to achieve. The low material thicknesses create processing challenges in injection moulding. For thin-walled internally coated split tubes according to concept 2, on the other hand, total wall thicknesses of up to less than 0.5 mm including CFRP reinforcement can be achieved. In addition, the elimination of the injection-moulded liner ensures economic savings potential. For these reasons, the decision was made to develop a can with an internal coating according to concept 2.

**Table 3** Concept comparison fiber composite can

| Features | 1a | 1b | 1c | 2 |
|---|---|---|---|---|
| Temperature resistance | + | + | + | + |
| Media resistance | + | + | + | + |
| Mechanical properties | + | + | + | + |
| Wall thickness | - | - | - | + |
| Processability | 0 | 0 | - | + |
| Economic efficiency | 0 | - | 0 | + |

The temperature and media resistance of the concept largely depends on the materials chosen. The evaluation in **Table 4** illustrates a comparison of various coatings.

**Table 4** Comparison of possible coating materials

| Features | Parylene | PVC | PA 6 | PPS | Epoxy resin |
|---|---|---|---|---|---|
| Costs | 0 | + | + | + | + |
| Temperature resistance | + | - | 0 | + | + |
| Media resistance | + | + | - | + | + |
| Tightness | - | + | + | + | 0 |
| Processability | - | 0 | + | + | - |

Parylene coatings, various thermoplastic materials and an epoxy resin, which is also used in fibre winding technology, were taken into consideration. The PPS material under consideration meets all important requirements for the can liner, so that this material was chosen. **Figure 13** shows a functional model of the newly developed FilaWin® can with PPS internal coating next to a series component with PPS injection-moulded liner. In direct comparison, the wall thickness of the new development is more than 50 % below that of the component manufactured according to concept 1a.

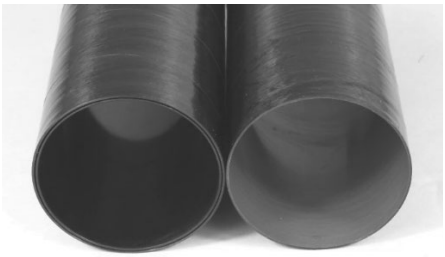

**Figure 13** Left: FilaWin® (concept 1a); Right: FilaWin® (concept 2, functional model)

# 5 Design of the functional Model and measurement

## 5.1 Functional model

To verify the simulation results, a functional model for realistic tests was built up and measured. During the entire measurement, the can from concept 2 was located between the stator and rotor stack and sealed them against each other. The rotor chamber was filled with liquid. Fig. 14 shows the measurement setup with the functional model.

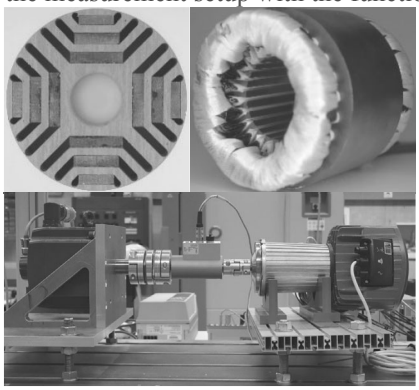

**Figure 14** Rotor of the PMSynRM (top left); Stator of the PMSynRM (top right); Measurement setup (below; pump unit with removed hydraulics on the right)

## 5.2 Electromotive Force (EMF)

Fig. 15, 16 shows the comparison of the measured and the simulated EMF at the rated speed of 3200 rpm in the time and frequency domain. It can be seen that in the time domain the sinusoidal curves have almost identical curves and the same amplitude. In the frequency domain, a minimal deviation of the fundamental waves (measurement 36.8 V and simulation 35.06 V) can be observed. This can be explained by a minimal difference between the magnetization characteristic curve of the electrical sheets stored in the simulation model and the real magnetization characteristic curve.

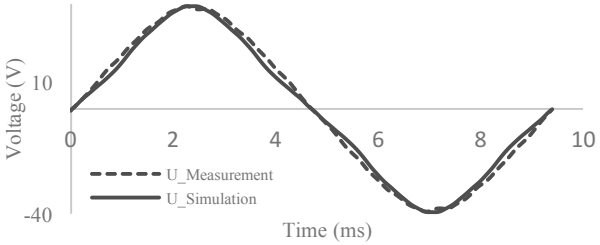


**Figure 15** EMF at 3200 rpm (time domain)

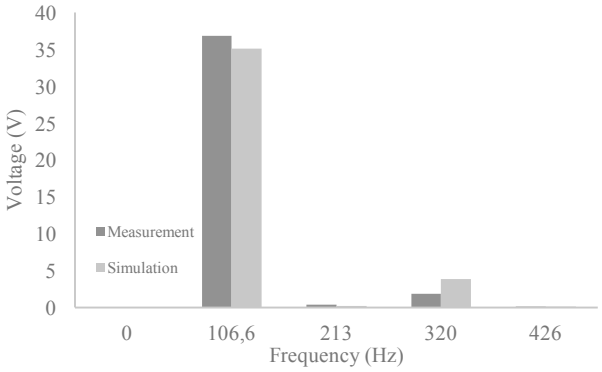


**Figure 16** EMF at 3200 rpm (frequency domain)

## 5.3 Comparison of simulation model, functional model and conventional permanent magnet synchronous motor

To prove the applicability of a PMSynRM as a component of an integrated drive system in a circulating pump, a functional model was developed, measured and compared with a commercially available product in permanent magnet synchronous motor design with NdFeB magnets (PMSM). In order to enable a good comparison, the external dimensions of the selected commercially available product had to be retained during the development of the functional model and a comparable efficiency had to be achieved.

Table 5 lists the differences between the simulated model, the functional model and the series product of an 800 Watt circulating pump. In the functional model, there are ferrite magnets in the flow barriers of the rotor and a can made of CFRP material as previously described. The PMSM uses rare earth magnets made of NdFeB and a can made of stainless steel. The construction volume of the PMSynRM is approx. 25 % larger than that of the PMSM, which is due to the, among other things, distributed winding in comparison to the tooth coil winding in the PMSM. The difference

in efficiency in rated operation between PMSM and PMSynRM is 2.3 percentage points.
The deviation of the efficiency between the simulation and the measurement of the PMSynRM is currently assumed to be a non-optimal current supply to the d- and q-axis by the standard frequency inverter.

**Table 5** Concept comparison

| Features | PMSynRM (Simulation) | PMSynRM | PMSM |
|---|---|---|---|
| Construction volume ($10^{-3}$ $m^3$) | 0,485 | 0,485 | 0,363 |
| Rated speed (rpm) | 3200 | 3200 | 3200 |
| Rated torque (Nm) | 2,4 | 2,4 | 2,4 |
| Air gap width (mm) | 1,25 | 1,25 | 1,38 |
| Winding | Distributed winding | Distributed winding | Tooth coil winding |
| Magnets | Ferrite | Ferrite | NdFeB |
| Can material | CFK | CFK | Stainless steel |
| Efficiency (%); Friction losses due to the pumped medium included | 81,7 | 79,7 | 82,0 |

# 6 Conclusion

On the basis of a SynRM, it was shown that the internal torque of the motor can be increased with the help of targeted filling of the flow barriers with ferrite magnets in the rotor. By adjusting the magnet volume in individual flux barriers, the undesired flux linkage $\Psi_q$ can be completely eliminated. Since the air gap in circulating pumps is increased by the can compared to dry-running motors, almost exclusively PMSM with rare-earth magnets are used there today. The presented development of a novel can has enabled the air gap of canned motors to be reduced by 50% compared with the state of the art. This now also enables the use of ferrite-supported synchronous reluctance motors as canned motor in circulating pumps. But it is not only through the use of PMSynRM that resource efficiency can be increased: Even with conventional PMSM, the reduced air gap allows the magnet volume and thus the costs to be reduced. The developed can is interesting for further applications, such as e-mobility. The power density can then be significantly increased with direct cooling of the stator.
In future work, the torque density and efficiency of PMSynRM will be further improved. The current supply to the windings is to be improved by optimized control. In addition, a functional model is currently being developed in which the flow barriers are completely ejected with ferrite magnets. It is also being investigated how the air gap field can be improved in tooth coil windings through targeted flux guidance in the stator, so that a reduction in installation space can be achieved with a simultaneous improvement in energy efficiency.

# 7 Literature


[1] J. Schuberth and F. Akkerman, “Die EG-Verordnung für die umweltgerechte Gestaltung von Umwaelzpumpen“, German Environment Agency, 2009

[2] Y. Burkhardt, G. Huth and S. Urschel, "Eddy current losses in PM canned motors," *The XIX International Conference on Electrical Machines - ICEM 2010*, Rome, 2010, pp. 1-7.

[3] B. Rieke at German Wikipedia, via Wikimedia Commons, https://de.wikipedia.org/wiki/Umwälzpumpe_(Heiztechnik), 22 May 2019

[4] Wilo SE, via Wikimedia Commons, https://commons.wikimedia.org/wiki/File:Pump_diagram.PNG, 22 May 2019

[5] N. Bianchi, "Synchronous reluctance and interior permanent magnet motors," *2013 IEEE Workshop on Electrical Machines Design, Control and Diagnosis (WEMDCD)*, Paris, 2013, pp. 75-84.

[6] T. A. Huynh, M. Hsieh, K. Shih and H. Kuo, "Design and analysis of permanent-magnet assisted synchronous reluctance motor," *2017 20th International Conference on Electrical Machines and Systems (ICEMS)*, Sydney, NSW, 2017, pp. 1-6.

[7] P. Niazi, H. A. Toliyat, Dal-Ho Cheong and Jung-Chul Kim, "A low-cost and efficient permanent magnet assisted synchronous reluctance motor drive," *IEEE International Conference on Electric Machines and Drives, 2005.*, San Antonio, TX, 2005, pp. 659-666.doi: 10.1109/IEMDC.2005.195794

[8] E. Schmidt, W. Brandl and C. Grabner, "Design improvement of synchronous reluctance machines with internal rotor flux barriers for high-speed drives," *2002 IEEE 33rd Annual IEEE Power Electronics Specialists Conference. Proceedings (Cat. No.02CH37289)*, Cairns, Qld., Australia, 2002, pp. 1949-1954 vol.4.

[9] S. Urschel and J. Dolgirev, "Energy- and resource saving synchronous reluctance machine for the use in circulation pumps," *2017 IEEE 3rd International Future Energy Electronics Conference and ECCE Asia (IFEEC 2017 - ECCE Asia)*, Kaohsiung, 2017, pp. 2139-2144.

[10] H. Schürmann, Konstruieren mit Faser-Kunststoff-Verbunden, Springer-Verlag Berlin Heidelberg, 2007.

[11] „Celanese Materials Database,“ Celanese, [Online]. Available: http://tools.celanese.com/, 09 May 2019



This work was supported by German Federal Ministry of Education and Research (BMBF), Berlin.